Fn-HMGB1 Adsorption Behavior Initiates Early Immune Recognition and Subsequent Osteoinduction of Biomaterials

*Qin Zhao, Zifan Zhao, Jing Zhang, Yueqi Ni, Simin Ouyang, Haoning Qi, Yiqian Yu, Richard J. Miron, Hua Tang, Yufeng Zhang**

Dr. Q. Zhao, Dr. J. Zhang, Dr. Y. Ni, Dr. S. Ouyang, Dr. H. Qi, Dr. Y. Yu and Prof. Y. Zhang

The State Key Laboratory Breeding Base of Basic Science of Stomatology (Hubei-MOST) & Key State Key Laboratory of Oral & Maxillofacial Reconstruction and Regeneration, Key Laboratory of Oral Biomedicine Ministry of Education, Hubei Key Laboratory of Stomatology, School & Hospital of Stomatology, Taikang Center for Life and Medical Sciences, Wuhan University, Wuhan 430079, China

Medical Research Institute, School of Medicine, Wuhan University, Wuhan, 430071, China

E-mail: zyf@whu.edu.cn

Dr. Z. Zhao,

Center of Digital Dentistry, Faculty of Prosthodontics, Peking University School and Hospital of Stomatology; National Center of Stomatology; National Engineeræing Research Center of Oral Biomaterials and Digital Medical Devices; Beijing Key Laboratory of Digital Stomatology; Research Center of Engineering and Technology for Computerized Dentistry Ministry of Health; National Clinical Research Center for Oral Diseases; Beijing, 100081, China

Prof. R. J. Miron

This article has been accepted for publication and undergone full peer review but has not been through the copyediting, typesetting, pagination and proofreading process, which may lead to differences between this version and the Version of Record. Please cite this article as doi: 10.1002/adhm.202301808.

WILEY-VCH

Department of Periodontology, University of Bern, Bern, Switzerland

Prof. H. Tang

Department of Rheumatology and Autoimmunology, Shandong Provincial Key Laboratory for Rheumatic Disease and Translational Medicine, The First Affiliated Hospital of Shandong First Medical University & Shandong Provincial Qianfoshan Hospital, Jinan, China

Institute of Infection and Immunity, Medical Science and Technology Innovation Center, Shandong First Medical University & Shandong Academy of Medical Sciences, Jinan, China

Keywords: biomaterial-associated molecular patterns, immune recognition, osteoinduction, protein adsorption, fibronectin

Abstract

Implantable biomaterials are widely used in bone tissue engineering, but little is still known about how they initiate early immune recognition and the initial dynamics. Herein, we attribute the early immune recognition and subsequent osteoinduction of biphasic calcium phosphate (BCP) after implantation to the protein adsorption behavior. By liquid chromatography tandem mass spectrometry (LC–MS/MS) analysis, we mapped the biomaterial related molecular patterns (BAMPs) formed after BCP implantation. Dominanted by the highly expressed extracellular matrix protein fibronectin (Fn) and the high mobility group box 1 (HMGB1). Then molecular dynamics (MD) simulations showed that Fn has the ability to bind more readily to the BCP surface than HMGB1. The preferential binding of Fn provided a higher adsorption energy for HMGB1. Furthermore, multiple hydrogen bonding sites between HMGB1 and Fn were demonstrated using a molecular docking approach. Ultimately, we obstructed the formation of BAMPs through HMGB1 antagonist glycyrrhizic

acid (GA), resulting in impaired immune recognition of myeloid differentiation factor 88 (MYD88) mediated dendritic cells (DCs) and macrophages (Mφs), as well as failed osteoinduction processes. This study introduces a mechanism for early immune recognition of implant materials based on proteins adsorption, providing perspectives for future design and application of tissue engineering materials.

1. Introduction

Bone substitutes or biomaterials have a wide range of medical applications and are a major means of addressing bone defects and promoting new bone formation[1]. However, there is a significant delay in the optimization and innovation of these biomaterials. Inhibiting immune response and improving biocompatibility are still the main thrusts of implantable bone substitutes. But evidence to the contrary shows that reckless suppression of the immune response will often lead to unfavorable tissue regeneration [2, 3]. Therefore, additional research is required to reveal the molecular mechanism of activating the immune response and initiating bone formation by biomaterials.

Immune response is one of the key factors in the osteoinduction of biomaterials and determines their ultimate fate [4]. In the molecular events preceding immune cell activation, the osteoinductive materials first undergo protein adsorption, which is ordered and follows molecular dynamics and structural dynamics principles [5, 6]. Protein adsorption is the first event that occurs at the biomaterial-tissue interface, which is critical for subsequent cellular behavior and further influences biomaterial-tissue interactions [7-10]. These processes determine to some extent the surface protein composition of the materials and its further biological effects. A recent study found that proteins adsorbed after implantation of

biomaterials form immune recognized motifs, known as "biomaterial related molecular patterns" (BAMPs), similar with pathogen-associated molecular patterns (PAMPs) or damage-associated molecular patterns (DAMPs) [11, 12]. However, the research on BAMPs is still in its Early-phase, and its internal structure is still unclear[13]. Therefore, the analysis and evaluation of the adsorption hierarchy of immune activation-related proteins on the surface of materials using molecular and structural dynamics methods can help to determine potential factors regarding the biomaterial to initiate immune recognition.

Biphasic calcium phosphate (BCP), a type of calcium phosphate ceramic, is a commonly used bone substitute in clinical practice and has received much attention for its osteoconductivity and partial osteoinductivity [14-16]. In recent years, many researchers have focused on the osteoimmunomodulatory properties of BCP and have further attempted material modifications. Interestingly, some have demonstrated that BCP ceramic often have contradictory effects in activating immune responses *in vitro* and *in vivo* [17, 18], and extensive or more complete blockade of the immune response after BCP implantation leads to failure of osteoinduction [19, 20]. This suggests that BCP has a unique performance advantage in the molecular events of protein adsorption processes that precede immune activation, but the mechanism is not clear.

Here, we present a model for the sequential adsorption of fibronectin (Fn) and high mobility group box 1 (HMGB1) on BCP to reveal the molecular mechanism of material-activated immune recognition to initiate new bone formation. First, RNA-seq showed that BCP activates immune recognition in the early phase (Day 7) and initiates osteoinduction in the late phase (Day 14). Furthermore, LC-MS/MS and ELISA showed that the key to BCP-activated immune recognition is the high aggregation of the danger signal protein HMGB1. Molecular dynamics (MD) simulation revealed more accessible binding sites of Fn on BCP than HMGB1, while the adsorption energy between HMGB1 and Fn was much higher than

that between it and the BCP surface. The molecular docking method was used to identify the interaction sites of HMGB1 with Fn. Noteworthy, we obstructed the formation of BAMPs through HMGB1 antagonist glycyrrhizic acid (GA) to allow for less adsorption of HMGB1 on the BCP, resulting in blocked myeloid differentiation factor 88 (MYD88)-mediated immune recognition of DCs and Mφs and failed osteoinduction. Our findings suggest that in BCP implantation environment, Fn-HMGB1 formed BAMPs that activated the early immune recognition and initiated osteoinduction process (**Scheme 1**). This work introduces a mechanism for early immune recognition of bone substitutes based on proteins adsorption, consolidating the knowledge and theory that immune response initiates tissue regeneration and providing perspectives for future design and application of tissue engineering materials.

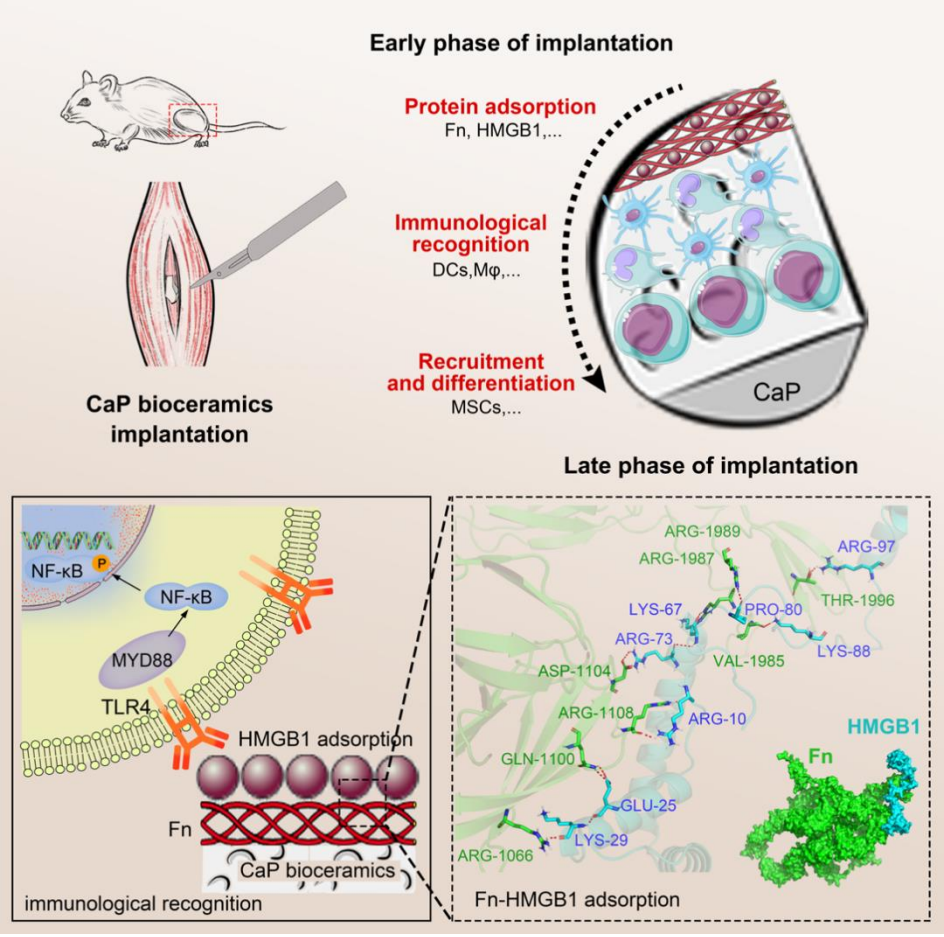

Scheme 1. Schematic representation of biomaterials adsorbing proteins that activate immune recognition and thus initiate regenerative reactions.

2. Results and Discussion

2.1 The recognition of biomaterials by the immune system is directly related to MSCs recruitment and osteoinduction

As a calcium phosphate ceramic, BCP has been widely demonstrated to be osteoinductive, and the BCP we used for implantation in the gastrocnemius muscle has been shown to be osteoinductive in previous studies [20-23]. While the bone defect environment is more indicative of the osteoinductive properties of the implant material [24, 25], embedding in the muscle better highlights the response of the immune system to the implant material [26-28]. Therefore, BCP implantation into the gastrocnemius muscle (**Figure 1**A) was suitable to reveal its molecular protein adsorption and immune response prior to osteoinduction (or exerting regenerative effects). X-ray diffraction (XRD) (Figure S1A) and scanning electron microscopy (SEM) micrographs (Figure S1B) were used to characterize BCP.

We observed the early biological process before BCP osteoinduction by RNAseq (early-phase at Day 7 and late-phase at Day 14). Gene Ontology (GO) enrichment analysis and Gene Set Enrichment Analysis (GSEA) showed that innate immune response and immune recognition signaling pathways, such as the MYD88-dependent TLR signaling pathway and NF-kappa B signaling pathway, were significantly upregulated at Early-phase (Figure 1B, C). The results of Kyoto Encyclopedia of Genes and Genomes (KEGG) enrichment analysis showed that the inflammation-related gene signaling pathway was significantly upregulated at Early-phase (Figure S2A, B). Other GSEA results also point to the dominance of early inflammatory and late regenerative processes (Figure S2C). Overall, the early

microenvironment of BCP implantation is dominated by an inflammatory response, while is predominantly late osteoinduction process. These two biological processes are inextricably linked, and the early inflammatory response may initiate late osteoinduction. This was also confirmed by Histological staining. DCs and Mφs are the predominant immune recognition cells, marked by F4/80 and CD11c, respectively [29-31]. IHC staining showed that immune recognition cells and TLR4/MYD88 pathway-related genes were more significantly expressed at Early-phase (Figure S3A, B, C, E, F). It is traditionally understood that DCs initiate foreign body immune recognition as dedicated antigen-presenting cells, mainly mediating the activation from innate to adaptive immunity [29]. Mφs also have a partial immune recognition role, mainly participating in inflammatory regulation and tissue regeneration induced by implantable materials in a differentially polarized manner with M1 and M2 [31, 32]. Combining our results confirms that both cells mediate material-induced immune recognition via TLR4/MYD88 signaling during the Early-phase of BCP implantation. During ectopic bone formation, MSCs are thought to be recruited by chemokines secreted by immune cells, such as CC-chemokine ligand 2 and 5 (CCL2, CCL5) and CXC-chemokine ligand 12 and 16 (CXCL12, CXCL16) [33, 34]. On the other hand, MSCs with osteogenic differentiation capacity are the cells most associated with ectopic ossification, marked by CD90 and CD105. IHC staining showed that MSCs were heavily enriched in the microenvironment at Late-phase (Figure S3D, G). It was found that inflammation was triggered at the Early-phase (Day 7), followed by stem cell recruitment (Late-phase, Day 14).

To verify the necessary connection between early inflammatory response and late osteoinduction process, we constructed the animal model with immune recognition system defects in vivo experiments. In previous studies, we have attempted to intervene in ectopic bone formation with BCP by modulating innate and adaptive immune responses through

multiple methods [20, 21, 23, 35]. However, in those studies, we interfered directly with the immune response to affect osteoinduction.

The widely used transgenic murine models LysM-DTA and CD11c-DTR + DT were used to achieve a deficiency in immune recognition cells (Mφs and DCs) in the microenvironment [36, 37]. MYD88-KO transgenic mice were used to block the TLR4/MYD88 signaling pathway [38]. HE staining and Masson staining showed that BCP in the WT group successfully showed osteoinductive effects but was not detected after blocking immune recognition. Similarly, immunohistochemical results showed that MSC recruitment was hindered after blocking immune recognition compared to the WT group (Figure 1D-F). These results convincingly confirm that the immune response induced by BCP implantation is essential for the subsequent osteoinduction.

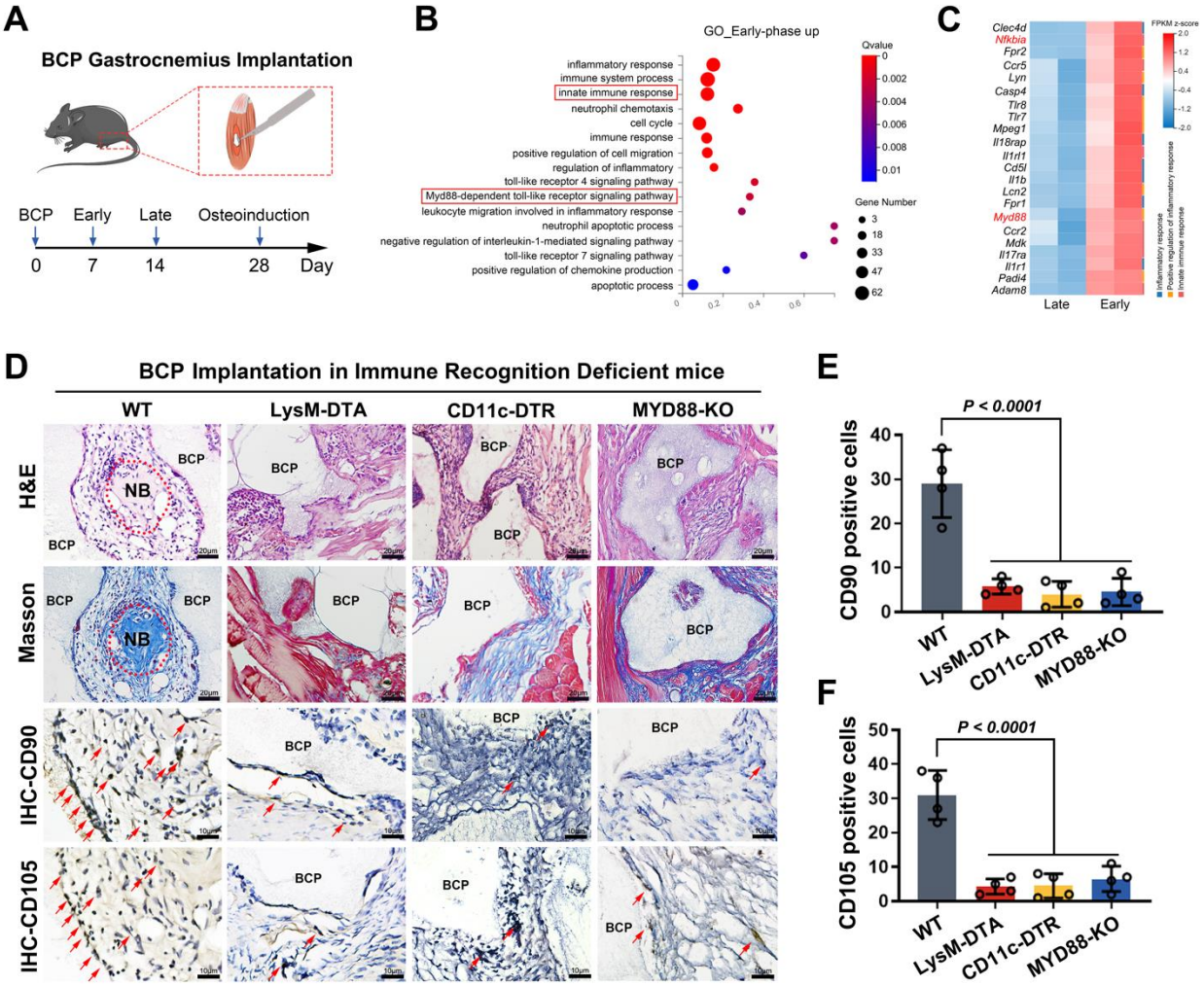

Figure 1. The recognition of biomaterials by the immune system is directly related to MSCs recruitment and osteoinduction. (A) Osteoinduction animal model of BCP implanted in mice gastrocnemius. (B) GO enrichment analysis of upregulated differential genes at Early-phase (Day 7). (C) Heatmaps of differential genes associated with immune response. (D) H&E and IHC staining illustrated that MSCs recruitment and osteoinduction were hindered in multiple immune recognition blocking models. (E-F) Quantitative analysis of (D). Positive cells were marked by red arrows, n=4.

2.2 BAMPs, formed by surface protein adsorption of biomaterials, activated the immune system

At present, how non-antigenic biomaterials initiate inflammation has been gradually concerned by researchers. Since the material itself has no immunogenicity and the implantation method has not changed the nature of the material itself, we then focused on what changes have occurred after the material is implanted into the body. To confirm the ability of BCP to initiate immune recognition early following implantation, we compared the immunogenicity between implanted BCP (imp-BCP) and BCP prior to implantation (pure-BCP). The imp-BCP was removed from the muscle at Early-phase after implantation to test its ability to activate immune recognition in vitro. Pure-BCP was used as a control. SEM showed the presence of adsorption substances on the surface of imp-BCP (**Figure 2**A). These adsorbed substances are mainly composed of adhesion proteins in the extracellular matrix and danger signals released due to surgical trauma [39, 40]. These components are a class of substances that are released into the extracellular matrix after stimulation of tissues or cells by factors such as injury and stress and can activate sterile inflammation through pattern recognition receptors such as Toll-like receptors or NOD-like receptors and are referred to as DAMPs [41]. A recent review suggests that the proteomic spectra of biomaterials adsorbed on their surfaces form complexes with immune activation effects, known as BAMP, similar to DAMP/PAMP[13]. To demonstrate whether the substances adsorbed onto the imp-BCP surface are immunogenic, Mφs and DCs were stimulated with extracted pure BCP and imp-BCP, and the activation ratio of immune recognition cells was detected using flow cytometry. The experiment was based on a single-species cell culture system *in vitro*, that is, the materials acted on Mφs and DCs separately. In the single-species Mφ culture system, we used CD86 as an indicator of its activation; in the single-species DC culture system, MHC II was used as an indicator of its activation. The results showed that the percentage of activation was greater after stimulation with imp-BCP than with pure BCP (Figure 2B, C). This indicates the presence of adsorbent substances in the extracted imp-BCP that activate the immune recognition signal, which is the main difference between imp-BCP and pure-BCP. Although

BCP can produce immunological effects through its granularity, porosity, surface crystal structure, ion release or degradation rate [42, 43], the substance adsorbed on its surface is the direct factor active in initiating endogenous immune recognition. At present, the understanding of BAMPs is still in its Early-phase, and its protein composition and hierarchical conformation are not clear. Subsequently, this study will take BCP as an example and focus on exploring the protein composition and hierarchical conformation of BAMPs.

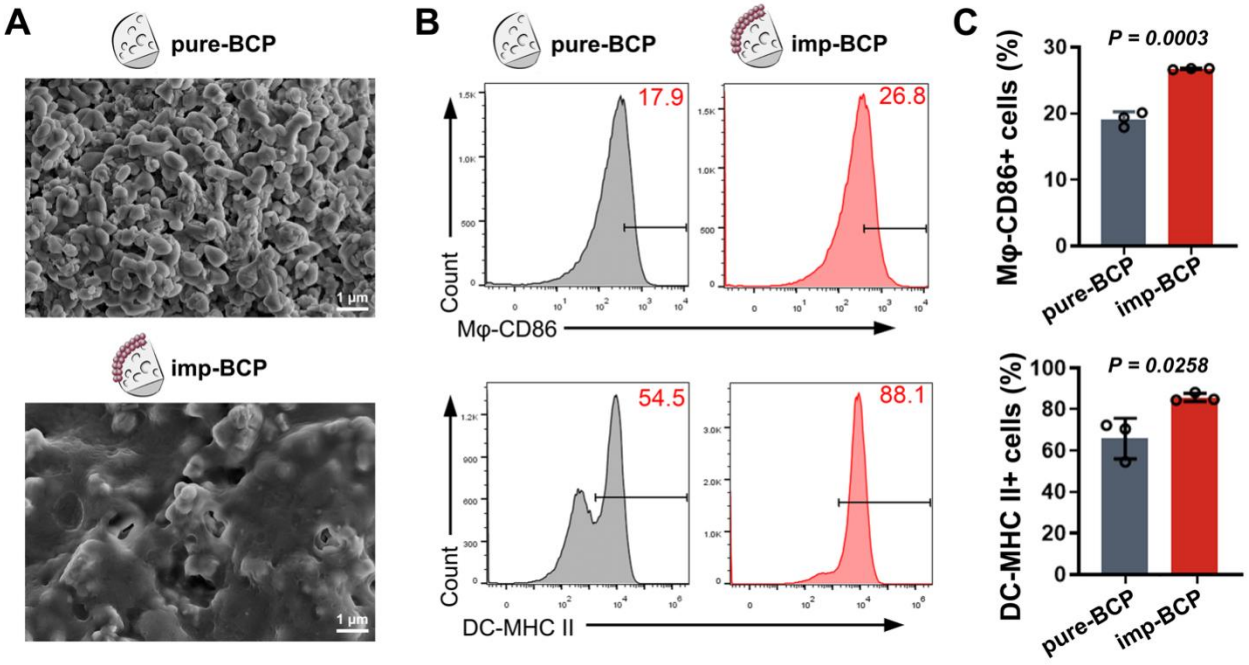

Figure 2. Imp-BCP with protein adsorption to initiate immune recognition in vitro. (A) Adsorption of imp-BCP and pure-BCP observed by SEM. (B) FACS showed that imp-BCP activates immune recognition rather than pure-BCP in vitro. (C) Quantification of positive cells in (B), n=3.

2.3 Detection and verification of BCP-BAMPs proteins

To further identify the key molecules of imp-BCP that initiate immune recognition, we performed a detailed analysis of the composition and content of the substances adsorbed on its surface. liquid chromatography tandem mass spectrometry (LC–MS/MS) is an essential tool for proteomics, facilitating the analysis of peptide mixtures in sample-limited situations [44]. The LC–MS/MS analysis was used to detect the proteins adsorbed on the imp-BCP. The functional annotation of LC–MS/MS analysis by KEGG and GO enrichment analysis showed that the function of adsorption proteins is associated with multiple immune or regenerative signaling pathways, including antigen processing and presentation and the chemokine signaling pathway (**Figure 3**A, B). According to the detailed sorting statistics conducted by Intensity, the results show that Fn and fibrinogen (Fg) are the main adsorbed proteins (Figure 3C). It is worth noting that HMGB1, as a danger signal protein that activates immune recognition, is another major protein adsorbed on imp-BCP (Figure 3C). The major source of HMGB1 is tissue injury and early inflammation, which can be translocated into the extracellular matrix upon cell death and directly initiate endogenous immune recognition [45]. From this, we hypothesize that HMGB1 adsorbs on the imp-BCP surface and may be the main agent leading imp-BCP triggering an immune response. In addition, to detect the concentration of adsorption proteins that are soluble in the solution and thus effectively stimulate immune cells, imp-BCP were eluted by PBS, and the protein concentration in the eluate was detected using ELISA. There were obvious advantages in the concentrations of HMGB1 and Fn (Figure 3D, E). The complete KEGG and GO enrichment analyses are presented in Figure S4 and Figure S5, respectively. This suggests that adhesion proteins, including HMGB1, are involved in multiple immune and regenerative processes. Subsequent HMGB1-related signaling pathways were analyzed by protein–protein interaction analysis, suggesting that HMGB1 activates the immune recognition process mainly through the TLR4/MYD88 signaling pathway (Figure S6). This conclusion was further confirmed by Western blot results, which showed that adding HMGB1 protein to the immune cell coculture

environment with BCP produced a stronger activation effect on TLR4/MYD88 signaling of immune cells (Figure 3F).

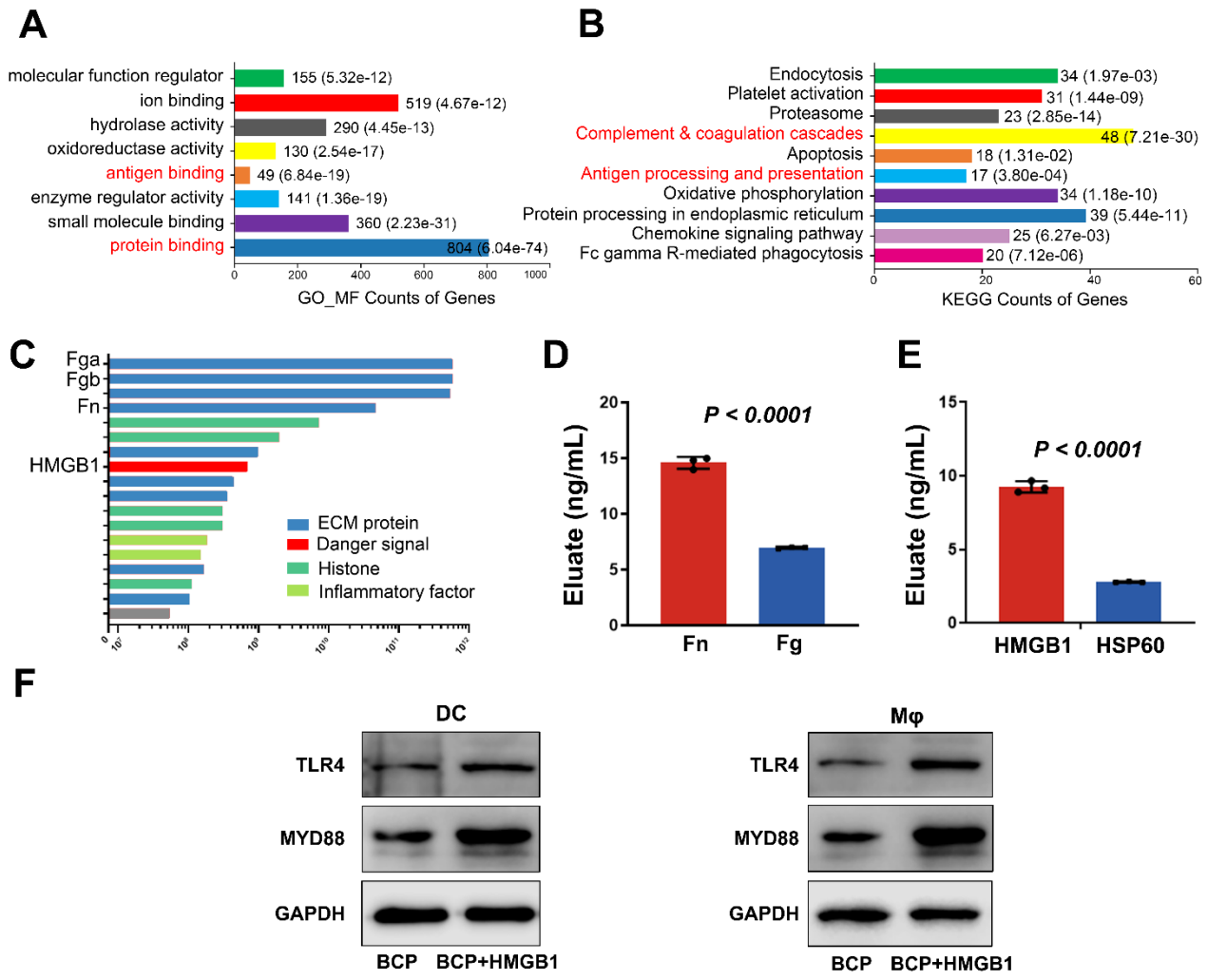

Figure 3. Detection and verification of adsorption protein on imp-BCP surfaces. (A-B) GO_MF and KEGG enrichment analysis of imp-BCP adsorption proteins observed by LC-MS/MS analysis. (C) Intensity of imp-BCP adsorption proteins observed by LC-MS/MS analysis. (D) ELISA of dominating ECM proteins in imp-BCP eluent, n=3. (E) ELISA of dominating danger signal in imp-BCP eluent, n=3. (F) HMGB1 activates the TLR4/MYD88 pathway in immune recognition cells in vitro detected by Western Blot.

2.4 Molecular dynamics simulations suggest that HMGB1 cannot be directly adsorbed onto the surface of calcium phosphate ceramic materials

Molecular dynamics simulations can be used to assess the conformational motion of one or more molecules, such as proteins and calcium phosphate ceramic, with details of interactions at the atomic level over time [46, 47]. After reaching equilibrium in solution, Fn and HMGB1 with calcium phosphate (CaP) ceramic surface models were placed in a unified virtual box according to a previous research method [48, 49]. The final system was used to simulate the adsorption of Fn and HMGB1 on CaP ceramic surfaces under experimental conditions (**Figure** 4A). The whole process was simulated in 10 ns, and RMSD results showed that the interaction between protein and CaP ceramics reached an equilibrium state at 2.5 ns (Figure S7A). The protein movement results revealed that Fn adsorbed to the CaP surface was closer and had a higher contact frequency than HMGB1 (Figure 4B, C). The analysis of the LJ potential energy showed that the CaP ceramic adsorption energy of Fn was higher than that of HMGB1 (Figure 4D). The coulomb force results are presented in (Figure S7B, C). These molecular dynamics results indicate that Fn has a stronger capacity than HMGB1 to adsorb onto the CaP ceramic surface. This suggested that HMGB1 has a weaker ability to bind directly to calcium phosphate ceramics compared to the adsorption protein Fn. In other words, HMGB1 is unable to bind directly to calcium phosphate ceramic materials in competition with strong adsorption proteins such as Fn. In the actual situation of BCP implantation in vivo, Fn showed a stronger occupation effect on the BCP surface.

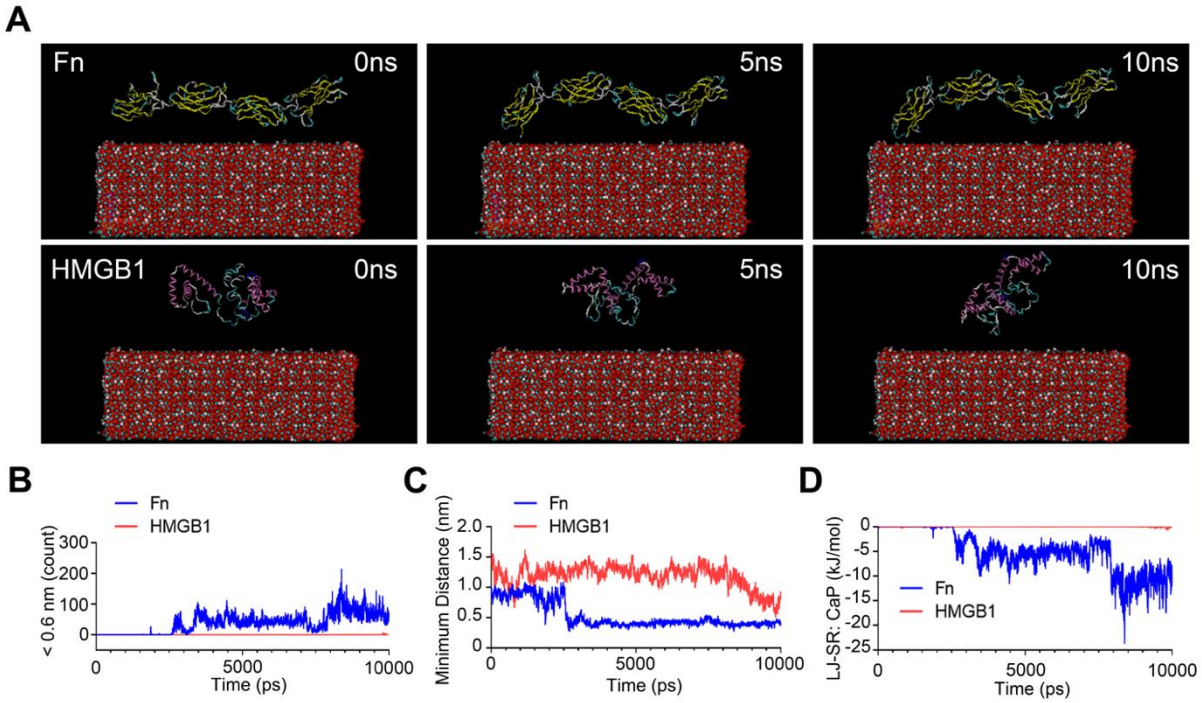

Figure 4. Molecular dynamics simulations suggest that HMGB1 cannot be directly adsorbed onto the surface of calcium phosphate ceramic materials. (A) The state of Fn and HMGB1 on CaP ceramics surfaces by GROMACS (0-10ns). (B) The count of contact distances <0.6nm between protein and CaP ceramic surface. (C) The minimum distance between protein and CaP ceramic surface. (D) LJ force between protein and CaP ceramic surfaces.

2.5 The sequential adsorption of Fn-HMGB1 on the BCP surface formed the hierarchical conformation of BAMPs

To further confirm whether there is an interaction between Fn and HMGB1 and to explore in what form the two are bound, molecular docking simulations were performed to identify the binding mode between HMGB1 and Fn. Molecular docking is a widely used virtual screening method that aims to predict the binding conformation of a small molecule ligand at a suitable target binding site [50]. Here, HMGB1 (blue, PDB entry 5ze0 chain N) and Fn (green, AlphaFold P11276) were selected for docking analysis. Figure 5 shows the superposition of

EAL domains in the substrate-bound conformation and the substrate-free conformation. The binding conformation shows that there is a tighter hydrogen bonding site between HMGB1 and Fn, which suggests that the adsorption of HMGB1 to calcium phosphate ceramics is achieved by binding to Fn on the surface of calcium phosphate ceramics (**Figure 5**A). The interaction sites are shown in (Figure 5B). Hydrogen bonding is based on electrostatic dipole–dipole interactions, including hydrogen donor and acceptor-acceptor-based dipoles, and is an important contribution to the free energy of biological macromolecules and macromolecular complexes [51, 52]. Compared to interaction with Fg, the interaction of HMGB1 with Fn had more sites of action, including hydrogen bonds, suggesting tighter binding of HMGB1 with Fn than with Fg. Accordingly, we speculated that there is Fn-HMGB1 ordered adsorption on the surface of calcium phosphate ceramics after implantation, which leads to the subsequent process of immune recognition and osteoinduction. The molecular docking simulation results of HMGB1 and Fg are shown in Figure S8. Since Fg is not the best adsorption medium for HMGB1, the results of Fg-related cytological experiments are not shown in this article. Furthermore, molecular dynamics was used to simulate the interaction between Fn and HMGB1, and (Figure S7D) shows that the simulated system has reached an equilibrium state. Molecular dynamics simulations of Fn and HMGB1 protein show a certain degree of interaction between them (Figure 5C). The contribution of each amino acid site in HMGB1 to the total energy of the interaction with Fn were shown in the (Figure 5D). A positive value represents the repulsive force, while a negative value represents the adsorption force. The horizontal axis represents the number of HMGB1 amino acids.

Molecular dynamics simulations and Molecular docking illustrated this conclusion, which still needs to be validated using real protein adhesion processes. BCP was immersed in protein solutions of Fn or HMGB1 to simulate the adsorption process, which were labeled the

BCP + Fn and BCP + HMGB1 groups, respectively. The two groups of BCP were subsequently mixed with Mφs and DCs, and the immune activation effect was detected by FACS. FACS results showed no significant activation of immune recognition cells in either group. The possible reason is that Fn can directly adsorb on the surface of BCP but has no activation effect on immune recognition cells. HMGB1 can activate immune recognition cells but cannot directly adsorb on the surface of BCP. Interestingly, however, when BCP was soaked with both Fn and HMGB1 protein solutions, a significant activation effect on immune recognition cells was observed (Figure 5E, F). In addition, fluorescently labeled Fn and HMGB1 proteins were used to verify adsorption capacity. As expected, Fn alone adsorbed more readily to the BCP surface than HMGB1 alone, whereas BCP with pre-adhered Fn made it easier for HMBG1 to adsorb to the surface (Figure S9A, B). It also matched previous results from molecular dynamics and molecular docking simulations. The above results indicate that Fn is necessary for the adsorption of HMGB1 onto BCP; therefore, we hypothesize that HMGB1 may be indirectly adsorbed onto the BCP surface via Fn. This is not the first time that Fn has been discovered as a medium for protein or cell adsorption onto materials. For cell adsorption, Fn was found to mediate the growth of HUVEC adhesion on polystyrene sodium sulfonate surfaces [53]. Similarly, Fn can also mediate the attachment of hMSCs on the surface of PEG hydrogels [54]. For protein interactions, Fn, as an extracellular matrix protein, has a broader and more important role in protein matrix assembly [55, 56].

This study discovered the typical BAMPs based on the protein composition and structure of Fn-HMGB1 sequential adsorption, through the study of BCP muscle implantation models.

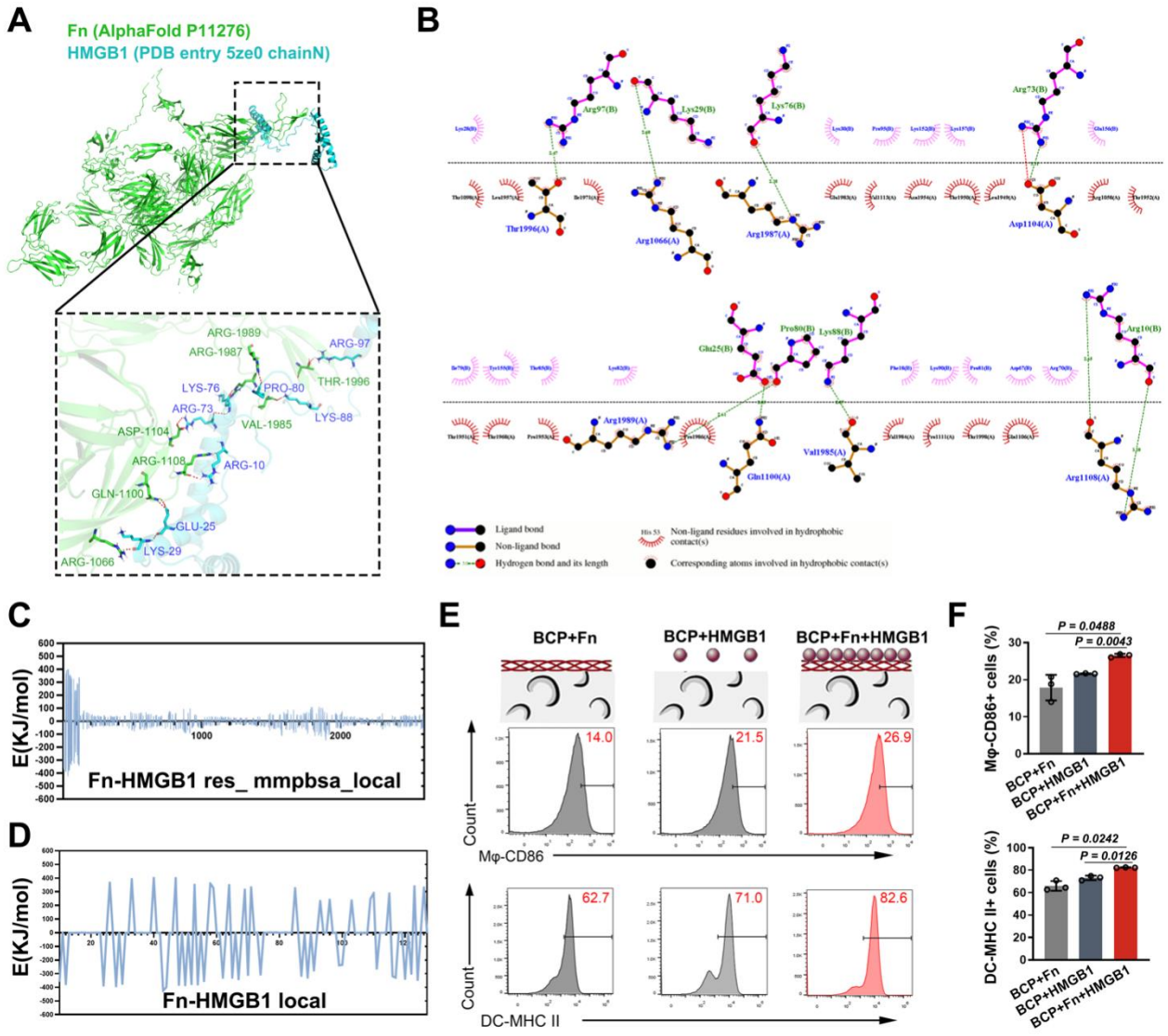

Figure 5. HMGB1 was indirectly adsorbed onto the surface of BCP by binding with Fn. (A) Molecular docking of HMGB1 (blue; PDB entry 5ZE0 chain N) and Fn (green; Alphahold P11276). (B) Interaction sites of HMGB1 and Fn. (C) Interaction energy of Fn and HMGB1. (D) The contribution of amino acid sites of HMGB1 to total energy. A positive value represents the repulsive force, while a negative value represents the adsorption force. The horizontal axis represents the number of HMGB1 amino acids. (E) FACS showed that Fn-HMGB1 sequential adsorption activates immune recognition in vitro. (F) Quantification of positive cells in (E), n=3.

2.6 Detected of BAMPs lead to failure of immune recognition and osteoinduction

Finally, we used the HMGB1 antagonist glycyrrhetinic acid (GA) to pre-soak BCP, aiming to neutralize soluble HMGB1 in tissues and disrupt the formation of BAMPs[57, 58]. And verify the immune activation and bone induction effects of BCP in this environment. Immunohistochemical staining showed that on the Early and Late-phase, compared with the control group, the GA group significantly reduced the number of cells activated by the immune recognition pathway (**Figure 6**A, D), and the number of MSCs around BCP significantly decreased (Figure 6B, E). Further, HE, Masson and IHC-COL1A1 staining showed that the osteoinduction capacity of BCP was limited after immersion in GA (Figure 6C, F), harvested at Day 28. This result shows that the complete structure of BAMPs is crucial for BCP immune recognition and osteoinduction process. The results of the aforementioned studies reveal a series of biological processes that occur after BCP implantation, which are summarized as follows: 1. HMGB1 appears in the tissue in free form due to surgical trauma. 2. After implantation of the material, the binding proteins Fn and Fg first adsorb to the BCP surface. 3. Solubility HMGB1 is indirectly adsorbed to the surface of BCP through multisite hydrogen bonding with Fn, forming BAMP and allow long-term retention. 4. Immune recognition cells (Mφs and DCs) recognize BCP with HMGB1 adsorption through the TLR4/MYD88/TRAF6/NFκB signaling pathway, and immune processes are initiated. 5. Immune activation promotes chemokine secretion and recruitment of MSCs, thereby initiating the organism's repair and osteoinduction process. BCP is a typical bone replacement scaffold with hydroxyapatite and β-tricalcium phosphate as main components, which is one of the CaP ceramic scaffolds with better osteoinductive effect [14-16]. These scaffold materials are biocompatible and have low immunogenicity. Therefore, they activate immune cells predominantly through early adsorption of proteins on their

surfaces, which are known as BAMPs [13]. In addition, the physicochemical properties of most CaP ceramic scaffold surfaces were similar, which determines that their patterns of protein adsorption are similar [59]. Although there are physicochemical differences between CaP ceramic scaffolds prepared by different processes, such differences are still insignificant compared to other biomaterials. Therefore, CaP ceramic scaffolds represented by BCP are likely to follow a similar protein adsorption pattern, based on which the design and modification of CaP ceramic scaffolds can be guided. While the protein adsorption pattern of other biomaterials needs to be further investigated.

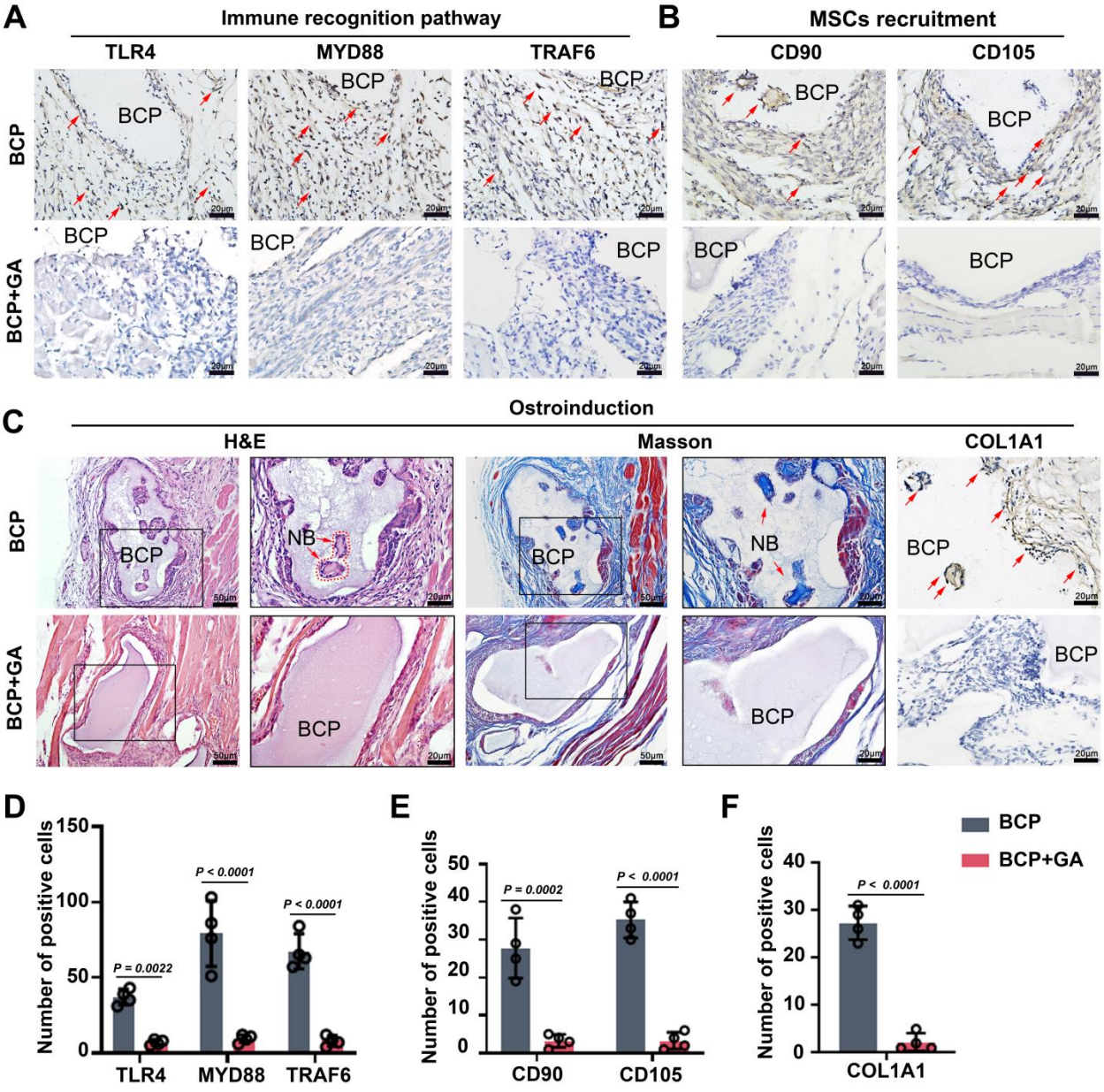

Figure 6. Detected of BAMPs lead to failure of immune recognition and osteoinduction. (A) Immune recognition was hindered in GA group. (B) MSCs recruitment was hindered in GA group. (C) Osteoinduction was hindered in GA group. (C-F) Quantitative analysis of IHC (A-C). Positive cells were marked by red arrows, n=4. GA: glycyrrhizic acid, NB: New Bone.

3. Conclusion

This study revealed the protein composition and conformation of BAMPs using LC-MS/MS, MD, and molecular docking methods. Combining in vivo and in vitro experiments, it innovatively elucidated the mechanism by which implanted materials initiate immune and regeneration processes. Binding proteins such as Fn were the first to adsorb to the BCP surface after implantation, while the danger signal HMGB1 bound to Fn and becomes enriched on the BCP surface through hydrogen bonding formed BAMPs. Subsequently, immune cells such as DCs and Mφs recognize the BAMPs through the MYD88 signaling pathway, initiating the immune response and participating in the regulation of the osteoinduction process. This study investigates the immune recognition of biomaterials from the perspective of Fn-HMGB1 sequential adsorption, reinforcing the important idea that immune recognition initiates the osteoinduction. It also provided an important basis for the optimization of tissue engineering materials.

4. Methods and materials

4.1 Preparation and characterization of BCP

The BCP granules were synthesized by a wet chemical precipitation method. BCP granules were prepared with HA/β-TCP at a ratio of 60/40, BCP granules had uniform specific surface area porosity, and irregular granules with 0.6 mm diameter were screened for implantation. XRD and SEM micrographs were used to characterize BCP.

4.2 Ethical Approval

The mice used in this study were handled in accordance with the policies of the Animal Research Ethics Committee of Wuhan University, Wuhan, China. Appropriate aseptic

conditions and anesthetic procedures were used throughout the procedure, and approval was obtained from the Institute of Biomedical Sciences Animal Use Ethics Committee according to protocol A31/2020.

4.3 Animals

4.3.1 Standardized model of BCP implanted into mice gastrocnemius muscle

Implantation experiments were performed on 8-week-old female mice. The large wound implantation method involves making an incision on the skin and muscle with a scalpel after preoperative hair removal. The incision was approximately 8 mm in length and was made with precision to avoid damaging the blood vessels. The BCP granules were inserted into the wound using ophthalmic forceps and sutured to the muscle layer and skin. For Figure 6, BCP was immersed in glycyrrhizic acid (GA, 10mM, MCE, HY-N0184) for 30 minutes before implantation.

4.3.2 Transgenic mouse

CD11c-DTR and MYD88-KO mice were obtained from Jackson Laboratory. The DC knockout group was injected with Diphtheria toxin (DT, 100 ng per mouse, Sigma, USA) one day before BCP implantation. LysM-DTA mice were hybridized from Rosa-DTA and LysM-CreER, obtained from The Jackson Laboratory.

4.4 RNA sequencing

For RNA-seq analysis, muscle around BCP was harvested at implantation Day 7 (Early-phase) and Day 14 (Late-phase), rinsed with PBS and frozen quickly in liquid nitrogen. Total RNA was extracted with TRIzol (TAKARA, Japan) and sequenced with the Illumina Platform. The project information submitted to SRA as BioProject PRJNA902907.

4.5 Histological staining

Muscle samples were collected for the preparation of paraffin sections, and samples were decalcified by immersing in EDTA solution and changing every two days for 3 weeks. Hematoxylin-eosin (H&E), Masson, and immunohistochemical (IHC) staining were performed according to the manufacturer's instructions (MXB biotechnologies, China). The primary antibodies were as follows: F4/80 (1:200, Abclonal, China), CD11c (1:200, Abclonal, China), TLR4 (1:200, Abclonal, China), MYD88 (1:200, Abclonal, China), TRAF6 (1:200, Abclonal, China), CCL5 (1:200, Abclonal, China), CD90 (1:200, Abclonal, China), CD105 (1:200, Abclonal, China), and COL1A1 (1:200, Abclonal, China).

4.6 Preparation of BCP eluent

BCP was implanted within the muscles of mice for 4 days, then euthanize the experimental animal and remove the intramuscular BCP. From each group, 0.5 g of BCP granules were soaked in 1mL sterile PBS solution and shaken at 37° for 24 hours. The eluate was aspirated with a 70 μm cartridge for cell experiments (Figure 2B) and ELISA (Figure 3D, E).

4.7 Cells

The Raw264.7 and DC2.4 cell lines were cultured in Dulbecco's modified Eagle’s medium (DMEM, HyClone, Germany) supplemented with 10% fetal bovine serum (FBS, HyClone, Germany), 100 U/mL penicillin G and 100 mg/mL streptomycin (HyClone, Germany) at 37 °C under humid conditions with 5% CO_2.

4.8 Flow cytometry

In Figure 2B and Figure 5E, cells were inoculated into 24-well plates and co-cultured with the corresponding group of sterile BCP granules or eluate for 24 hours at a cell density of 80%. Thereafter, single cell suspensions were prepared. Cells were incubated with antibodies

for 30 minutes at 4 °C, protected from light, using the following antibodies: IA/IE-PE594 (1:200, Biolegend, U.S.A.), and CD86-APC (1:200, Biolegend, U.S.A.). Flow cytometry was performed using a Cytoflex flow cytometer, and data were analyzed using FlowJo10.

4.9 liquid chromatography tandem mass spectrometry (LC–MS/MS)

Testing was performed according to the method provided by BiotechPack Scientific (China). Briefly, samples were first subjected to SDS–PAGE and decolorized after cutting the corresponding gel strips. Then, the decolorized gel pellets were subjected to trypsin enzymatic digestion, after which the processed samples were analyzed by LC–MS/MS to obtain raw files of the original mass spectrometry results. Results were analyzed by MaxQuant (1.6.2.10) software to match the data and obtain the identification results.

4.10 Enzyme-linked immunosorbent assay (ELISA)

The ELISA protocol followed the steps provided in the kits HMGB1 (MU30043, Bioswamp, China), HSP-60 (MU30603, Bioswamp, China), Fn (MU30179, Bioswamp, China), and Fg (MU30331, Bioswamp, China). The BCP eluent tested is described in detail in 4.6.

4.11 Western blot

Protein extraction and separation by sodium dodecyl sulfate–polyacrylamide gel electrophoresis (SDS–PAGE) were performed according to a previous method [20, 22]. The primary antibodies were anti-TLR4 (1:1000, Abclonal, China), anti-MYD88 (1:1000, Abclonal, China), and anti-GAPDH (1:5000, Abclonal, China). The membranes were incubated with secondary antibodies (1:6000, BioSharp, China) and the results were visualized by WesternBright ECL HRP Substrate Kit (Advansta, USA) at last.

4.12 Molecular dynamics

According to previous studies [49], the molecular dynamics simulations of protein adhesion were performed by the GROMACS 2016.4 package with the charmm36 force field. The 3D structures of HMGB1 and FN-III_{9-10} were obtained from the Protein Data Bank (PDB ID: 5ZE0; PDB ID: 1FNF). The CaP ceramics surface was built by Material Studio 8.0 and the (001) surface of hydroxyapatite was adopted. The basic model was originally built in a cubic box with a size of 19.1 * 9.6 * 16 nm^3 and the simulation box was solvated with SPC water molecules. The Na^+ ions were added to neutralize the systems. The steepest descent method was adopted for energy minimization. Systems were heated to 323 K using the V-rescale thermostat in the NVT ensemble for 100 ps and equilibrated for 1 ns in NPT. Then, a 10 ns molecular dynamics simulation for protein-surface interaction was performed. The VMD software was used for visualization and data analysis.

4.13 Molecular docking

The 5ZE0 chain N was used to represent HMGB1 structure, and the missing residues were filled in using modeler 9.23. The docking software hdock was used, and the docking sites were searched using global mode. The plots shown in Figure 5A and Supplementary Figure 8A-C were plotted by PyMOL, and those shown in Figure 5B and Supplementary Figure 8D, E were plotted by LigPlot+.

4.14 Protein adsorption and functional assays in vitro

In Figure 5E-F, BCP were immersed separately or sequentially in fluorescently labeled Fn (20μg/mL) and HMGB1 (50μg/mL) for 2 minutes, followed by gentle rinsing with 200μL PBS. The treated BCP were used to co-culture with DCs and macrophages for 24 hours, followed by analysis of the cells using flow cytometry. In Figure S9, the fluorescently labeled Fn (488) and HMGB1 (594) were used to immerse BCP and analyze the fluorescence intensity on the BCP surface under upright fluorescence microscope.

4.15 Statistical analysis

All data were statistically analyzed using Prism 8 (GraphPad Software Co., San Diego, CA, USA). All results were presented as means ± standard deviations. Sample size (n) for each statistical analysis can be found in the figure legends and statistical graphs. The Student's t-test was used for comparisons between two groups. A one-way analysis of variance followed by the Tukey multiple-comparison post-test was performed for comparisons between more than two groups. A P-value of <0.05 was considered statistically significant.

Acknowledgements

Qin Zhao, Zifan Zhao and Jing Zhang contributed equally to this work. This work is supported by the National Natural Science Foundation of China (82025011, 82270981, 82100975).

Conflict of Interest

The authors declare no conflict of interest.

References

[1] Y. Fillingham, J. Jacobs, *Bone Joint J* **2016**, 98-B, 6.

[2] J. M. Anderson, A. Rodriguez, D. T. Chang, *Semin Immunol* **2008**, 20, 86.

[3] S. A. Eming, *Semin Immunol* **2014**, 26, 275.

[4] M. Tsukasaki, H. Takayanagi, *Nat Rev Immunol* **2019**, 19, 626.

[5] P. Thevenot, W. Hu, L. Tang, *Curr Top Med Chem* **2008**, 8, 270.

[6] M. R. Wilkins, J. C. Sanchez, A. A. Gooley, R. D. Appel, I. Humphery-Smith, D. F. Hochstrasser, K. L. Williams, *Biotechnol Genet Eng Rev* **1996**, 13, 19.

[7] F. Deng, W. Zhai, Y. Yin, C. Peng, C. Ning, *Bioact Mater* **2021**, 6, 208.

[8] C. Linsley, B. Wu, B. Tawil, *Tissue Eng Part A* **2013**, 19, 1416.

[9] S. Danmark, A. Finne-Wistrand, A. C. Albertsson, M. Patarroyo, K. Mustafa, *Biomed Mater* **2012**, 7, 035011.

[10] W. Lu, W. Duan, Y. Guo, C. Ning, *J Biomater Appl* **2012**, 26, 637.

[11] J. E. Babensee, *Semin Immunol* **2008**, 20, 101.

[12] M. N. Abdallah, S. D. Tran, G. Abughanam, M. Laurenti, D. Zuanazzi, M. A. Mezour, Y. Xiao, M. Cerruti, W. L. Siqueira, F. Tamimi, *Acta Biomater* **2017**, 54, 150.

[13] S. Wang, Y. Chen, Z. Ling, J. Li, J. Hu, F. He, Q. Chen, *Int J Oral Sci* **2022**, 14, 52.

[14] X. Chen, M. Wang, F. Chen, J. Wang, X. Li, J. Liang, Y. Fan, Y. Xiao, X. Zhang, *Acta Biomater* **2020**, 103, 318.

[15] M. U. Munir, S. Salman, A. Ihsan, T. Elsaman, *Int J Nanomedicine* **2022**, 17, 1903.

[16] Q. Zhu, T. Chen, J. Xia, D. Jiang, S. Wang, Y. Zhang, *J Biomater Appl* **2022**, 37, 600.

[17] K. Qi, N. Li, Z. Zhang, G. Melino, *Cell Immunol* **2018**, 326, 86.

[18] P. Humbert, M. A. Brennan, N. Davison, P. Rosset, V. Trichet, F. Blanchard, P. Layrolle, *Front Immunol* **2019**, 10, 663.

[19] O. I. Eseonu, C. De Bari, *Rheumatology (Oxford)* **2015**, 54, 210.

[20] Z. Zhao, Q. Zhao, B. Gu, C. Yin, K. Shen, H. Tang, H. Xia, X. Zhang, Y. Zhao, X. Yang, Y. Zhang, *Theranostics* **2020**, 10, 3533.

[21] Q. Zhao, M. Shi, C. Yin, Z. Zhao, J. Zhang, J. Wang, K. Shen, L. Zhang, H. Tang, Y. Xiao, Y. Zhang, *Nanomicro Lett* **2020**, 13, 28.

[22] C. Yin, X. Jia, Q. Zhao, Z. Zhao, J. Wang, Y. Zhang, Z. Li, H. Sun, Z. Li, *Mater Sci Eng C Mater Biol Appl* **2020**, 110, 110671.

[23] J. Zhang, Q. Wu, C. Yin, X. Jia, Z. Zhao, X. Zhang, G. Yuan, H. Hu, Q. Zhao, *J Leukoc Biol* **2021**, 110, 485.

[24] Z. M. Johnson, Y. Yuan, X. Li, T. Jashashvili, M. Jamieson, M. Urata, Y. Chen, Y. Chai, *Stem Cells Transl Med* **2021**, 10, 1170.

[25] C. Susin, J. Lee, T. Fiorini, K. T. Koo, P. Schupbach, P. D. M. Angst, A. Finger Stadler, U. M. Wikesjo, *J Clin Periodontol* **2018**, 45, 884.

[26] L. Cheng, A. T. Khalaf, T. Lin, L. Ran, Z. Shi, J. Wan, X. Zhou, L. Zou, *Metabolites* **2020**, 10.

[27] L. Cheng, Z. Liu, S. Yan, Z. Chen, L. Zou, Z. Shi, *Biomed Mater Eng* **2019**, 30, 287.

[28] B. H. Fellah, N. Josselin, D. Chappard, P. Weiss, P. Layrolle, *J Mater Sci Mater Med* **2007**, 18, 287.

[29] C. Thery, S. Amigorena, *Curr Opin Immunol* **2001**, 13, 45.

[30] S. C. Knight, A. J. Stagg, *Curr Opin Immunol* **1993**, 5, 374.

[31] S. W. Kashem, M. Haniffa, D. H. Kaplan, *Annu Rev Immunol* **2017**, 35, 469.

[32] C. M. Wilke, I. Kryczek, W. Zou, *Int Rev Immunol* **2011**, 30, 120.

[33] B. S. Hill, A. Pelagalli, N. Passaro, A. Zannetti, *Oncotarget* **2017**, 8, 73296.

[34] Y. Shi, L. Du, L. Lin, Y. Wang, *Nat Rev Drug Discov* **2017**, 16, 35.

[35] J. Wang, Q. Zhao, L. Fu, S. Zheng, C. Wang, L. Han, Z. Gong, Z. Wang, H. Tang, Y. Zhang, *Bioact Mater* **2022**, 15, 446.

[36] L. Pan, P. Bai, X. Weng, J. Liu, Y. Chen, S. Chen, X. Ma, K. Hu, A. Sun, J. Ge, *Circulation* **2022**, 145, 659.

[37] C. L. Bennett, B. E. Clausen, *Trends Immunol* **2007**, 28, 525.

[38] J. Y. Lim, Y. K. Lee, S. E. Lee, J. M. Ju, K. S. Eom, Y. J. Kim, N. G. Chung, D. C. Jeong, G. Park, E. Y. Choi, C. K. Min, *Mucosal Immunol* **2016**, 9, 730.

[39] J. M. Anderson, T. L. Bonfield, N. P. Ziats, *Int J Artif Organs* **1990**, 13, 375.

[40] C. J. Wilson, R. E. Clegg, D. I. Leavesley, M. J. Pearcy, *Tissue Eng* **2005**, 11, 1.

[41] T. Gong, L. Liu, W. Jiang, R. Zhou, *Nat Rev Immunol* **2020**, 20, 95.

[42] Z. Chen, A. Bachhuka, F. Wei, X. Wang, G. Liu, K. Vasilev, Y. Xiao, *Nanoscale* **2017**, 9, 18129.

[43] Z. Chen, S. Ni, S. Han, R. Crawford, S. Lu, F. Wei, J. Chang, C. Wu, Y. Xiao, *Nanoscale* **2017**, 9, 706.

[44] M. Gaspari, G. Cuda, *Methods Mol Biol* **2011**, 790, 115.

[45] G. Chen, M. F. Ward, A. E. Sama, H. Wang, *J Interferon Cytokine Res* **2004**, 24, 329.

[46] T. A. Collier, T. J. Piggot, J. R. Allison, *Methods Mol Biol* **2020**, 2073, 311.

[47] R. Lazim, D. Suh, S. Choi, *Int J Mol Sci* **2020**, 21.

[48] H. Qi, M. Shi, Y. Ni, W. Mo, P. Zhang, S. Jiang, Y. Zhang, X. Deng, *Adv Healthc Mater* **2021**, 10, e2100994.

[49] F. Zhang, H. Qi, W. Mo, Y. Ni, Q. Zhao, Y. Wang, S. Jiang, Q. Tang, Y. Cheng, X. Xiao, Y. Zhang, *Adv Healthc Mater* **2022**, 11, e2200382.

[50] D. Dong, Z. Xu, W. Zhong, S. Peng, *Curr Top Med Chem* **2018**, 18, 1015.

[51] A. V. Morozov, T. Kortemme, *Adv Protein Chem* **2005**, 72, 1.

[52] E. Nittinger, T. Inhester, S. Bietz, A. Meyder, K. T. Schomburg, G. Lange, R. Klein, M. Rarey, *J Med Chem* **2017**, 60, 4245.

[53] M. Najab-Benhayoun, H. Serne, M. Jozefowicz, A. M. Fischer, C. Brisson, Y. Sultan, *J Biomed Mater Res* **1993**, 27, 511.

[54] N. R. Gandavarapu, P. D. Mariner, M. P. Schwartz, K. S. Anseth, *Acta Biomater* **2013**, 9, 4525.

[55] P. Singh, C. Carraher, J. E. Schwarzbauer, *Annu Rev Cell Dev Biol* **2010**, 26, 397.

[56] C. J. Dalton, C. A. Lemmon, *Cells* **2021**, 10.

[57] Y. Wang, H. Zhang, Q. Chen, F. Jiao, C. Shi, M. Pei, J. Lv, H. Zhang, L. Wang, Z. Gong, *Cell Prolif* **2020**, 53, e12829.

[58] C. Liu, T. Hu, Z. Cai, Q. Xie, Y. Yuan, N. Li, S. Xie, Q. Yao, J. Zhao, Q. Q. Wu, Q. Tang, *Front Cell Dev Biol* **2020**, 8, 713.

[59] W. H. Lee, C. Y. Loo, R. Rohanizadeh, *Colloids Surf B Biointerfaces* **2014**, 122, 823.

Journal's Table of Contents (ToC)

Short text

It revealed the sequential adsorption of Fn and HMGB1 on BCP scaffolds using LC-MS/MS, MD, and molecular docking methods. Combining in vivo and in vitro experiments, it elucidated the mechanism by which implanted BCP initiate immune and regeneration processes. It investigated the immune recognition of biomaterials from the perspective of Fn-HMGB1 adsorption, reinforcing the view that immune recognition initiates osteoinduction.

Eye-catching figure

WILEY-VCH